Tellus (1984), *36A*, 21–29

Static initialization of primitive equation models on a bounded, extratropical region

By TROND IVERSEN, *Norwegian Institute for Air Research, P.O. Box 130, N-2001 Lillestrøm, Norway* and THOR ERIK NORDENG, *The Norwegian Meteorological Institute, P.O. Box 320, Blindern, Oslo 3, Norway*

(Manuscript received May 5, 1982; in final form March 16, 1983)

ABSTRACT

Two filtered models (FM) are studied for their properties in providing initial data for primitive equation models (PEM) solved on a bounded, extratropical region. The methods are tested on actual data, and topography and friction are included. The results suggest that filtered models are powerful tools for suppressing gravity-inertia waves in the primitive equation models in cases where the horizontal normal modes are difficult to find. Inconsistencies between the initialization method and the prognostic model regarding vertical, finite differences and horizontal approximations at the lateral boundaries, may give rise to low-frequency "noise". Inconsistent horizontal, finite differences chiefly give rise to high-frequency "noise" that can be removed by a time filtering technique.

1. Introduction

The primitive equations governing the large-scale atmospheric motion are the hydrodynamic equations of motion modified by the quasi-hydrostatic approximation. The general solution to this set of equations describes a wide range of physical phenomena. In this paper, the *Rossby mode* of the solution signifies an advective type flow of small Rossby number, while the *gravity mode* consists of Lamb waves and gravity-inertia waves. Leith (1980) demonstrated that a general state uniquely decomposes into a Rossby mode state and a gravity mode state of the system linearized about a state at rest.

It is well known that the initial conditions for the primitive equations must be carefully chosen to avoid an amount of gravity mode energy that will ruin the forecast. Filtered models were early proposed as a tool to compute the required balance between the mass and wind field (Hinkelmann, 1951; Charney, 1955; Phillips, 1960). This approach is called *static initialization.* It was quite early discarded owing to a number of reasons. The method is hardly applicable in the tropics without special treatments (see Houghton and Washington, 1969). Furthermore, physical processes are difficult to incorporate in the procedure. Finally, the diagnostic equations applied are generally formulated so as to be inconsistent with the primitive equations.

To dispense with some of these problems, the method of *dynamic initialization* was introduced instead (Miyakoda and Moyer, 1968; Nitta and Hovermale, 1969). In this method, the primitive equations are integrated back and forth about the initial time step utilizing the geostrophic adjustment process. The adjustment is accelerated by the use of high-frequency damping devices. Unfortunately, this damping also destroys some of the Rossby mode energy, since it does not distinguish between small-scale synoptic features and large-scale, or high-order, gravity waves. Another drawback is that the convergence of the iteration procedure is uncertain and time consuming. In a recent paper by Bratseth (1982), some of these problems seem to be eliminated.

A recent approach to the initialization problem is the *non-linear normal mode initialization* (Machenhauer, 1977; Baer, 1977; Baer and Tribbia, 1977). The Machenhauer scheme, that claims the time rate of change of the normal mode coefficients for the gravity mode to vanish, was employed in the ECMWF model (Temperton and Williamson, 1979). The Baer–Tribbia scheme, which is somewhat more general, was tested by Tribbia (1979). The latter paper emphasizes the method's applicability in the tropics. The main problem with this method is that it requires detailed knowledge of the horizontal and vertical modes of the linearized system. For most limited area models, the horizontal modes are hardly possible to find. Another problem is the lack of convergence for high-order vertical modes and for when physical processes are included (Temperton and Williamson, 1979).

In this paper we wish to re-examine the static initialization method applied on a bounded, extratropical domain, to investigate how serious the above-mentioned problems appear to be in practice. Leith (1980) showed that in an f-plane model, the first iteration step in the Baer–Tribbia and Machenhauer schemes corresponds exactly to the solution of the non-linear balance equation with a divergent wind component computed from the quasi-geostrophic omega equation. This has been shown earlier by linear theory (Phillips, 1960) to be the required divergence to completely filter the gravity mode. Such a method of static initialization was tested by Lejenäs (1977), showing rather discouraging results; it will nevertheless be employed here. A more complete filtered model from the Lorenz (1960) energy consistent hierarchy will also be considered. The filtering approximation of this latter model is that the time rate of change of the horizontal divergence vanishes. This is in many ways similar to the filtering condition of the Machenhauer scheme, and is therefore an interesting approach. We will employ a height-constrained method, i.e. the wind field is adjusted to the mass field. To satisfy the condition for ellipticity of the non-linear balance equation, the analysed mass field must be modified in some areas. This problem is also encountered in height-constrained, non-linear normal mode initialization (Daley, 1978; Tribbia, 1981).

In the experiments, standard pressure coordinates are used and topography and Ekman friction are parameterized. The filtered models are described in Section 2, the primitive equation models and the experiments in Section 3 and the experimental results in Section 4.

2. The initialization methods

We have solved two filtered models to obtain the horizontal wind from the analysed mass field. In both models, the horizontal wind is split into a rotational and a divergent part:

$$\mathbf{v} = \mathbf{v}_\psi + \mathbf{v}_\chi, \tag{2.1}$$

where $\mathbf{v}_\psi = \mathbf{k} \times \nabla\psi$ and $\mathbf{v}_\chi = \nabla\chi$. Here $\mathbf{v}$ is the horizontal wind, ψ the stream function, χ the velocity potential, $\mathbf{k}$ the vertical unit vector and ∇ the horizontal gradient at constant pressure.

The equations are:
the balance equation (solved for ψ):

$$\nabla^2\phi - \nabla\cdot(f\nabla\psi) + \nabla\cdot(\mathbf{v}_\psi\cdot\nabla\mathbf{v}_\psi) + a\Big\{\mathbf{v}_\psi\cdot\nabla(\nabla^2\chi) + 2\nabla\cdot(\mathbf{v}_\chi\cdot\nabla\mathbf{v}_\psi) + \nabla\cdot\left(\omega\frac{\partial\mathbf{v}_\psi}{\partial p}\right)\Big\} = 0; \tag{2.2}$$

the omega equation (solved for ω):

$$\begin{aligned}\nabla^2(S\omega) + f^2\omega_{pp} = {} & f\frac{\partial}{\partial p}[\mathbf{v}_\psi\cdot\nabla(\nabla^2\psi + f)] \\ & - \nabla^2(\mathbf{v}_\psi\cdot\nabla\phi_p) + a\Big\{\frac{\partial}{\partial t}\frac{\partial}{\partial p}[\nabla\cdot(\mathbf{v}_\psi\cdot\nabla\mathbf{v}_\psi)] \\ & - \frac{\partial}{\partial t}\frac{\partial}{\partial p}\nabla f\cdot\nabla\psi + \frac{\partial}{\partial p}[\mathbf{v}_\chi\cdot\nabla(\nabla^2\psi + f)] \\ & - \nabla^2(\mathbf{v}_\chi\cdot\nabla\phi_p) + f\omega\nabla^2\psi_{pp} - f\omega_{pp}\nabla^2\psi \\ & + f\frac{\partial}{\partial p}(\mathbf{k}\cdot\nabla\omega\times\mathbf{v}_{\psi_p}) + f\frac{\partial}{\partial p}(\mathbf{k}\cdot\nabla\omega\times\mathbf{v}_{\chi_p}) \\ & + 2\frac{\partial}{\partial p}[\nabla\cdot(\mathbf{v}_\chi\cdot\nabla\mathbf{v}_{\psi_t})] + \frac{\partial}{\partial p}(\nabla\omega\cdot\mathbf{v}_{\psi_{pt}}) \\ & - \frac{\partial}{\partial p}[\mathbf{v}_{\psi_t}\cdot\nabla\omega_p]\Big\};\end{aligned} \tag{2.3}$$

the continuity equation (solved for χ):

$$\nabla^2\chi + \omega_p = 0; \tag{2.4}$$

the vorticity equation (solved for ψ_t):

$$\begin{aligned}&\nabla^2\psi_t + \mathbf{v}_\psi\cdot\nabla(\nabla^2\psi + f) \\ &\quad - f\omega_p + a\{\mathbf{v}_\chi\cdot\nabla(\nabla^2\psi + f) - \omega_p\nabla^2\psi \\ &\quad + \omega\nabla^2\psi_p + \mathbf{k}\cdot\nabla\omega\times\mathbf{v}_p\} = 0.\end{aligned} \tag{2.5}$$

The symbols are standard except for the vertical, static stability parameter $S = -\alpha\theta_p/\theta$.

If the tracer a is equal to zero, we have the classical non-linear balance equation and the quasi-geostrophic omega equation which corresponds to the first step in the Machenhauer iteration. Here, this model is called FM1. The model FM2 is achieved when $a = 1$. The filtering approximation is

$$\frac{\partial}{\partial t} \nabla^2 \chi = 0. \tag{2.6}$$

The upper and lower boundary conditions are

$$\omega = 0 \quad \text{at} \quad p = 200\,\text{mb}, \tag{2.7a}$$

and

$$\omega = \rho_s \left[f \frac{\partial \psi_0}{\partial t} - g\mathbf{v}_0 \cdot \nabla H - f^{-1} g C_D |\mathbf{v}_s| \mathbf{k} \cdot \nabla \times \mathbf{v}_s \right] \quad \text{at} \quad p = 1000\,\text{mb} \tag{2.7b}$$

with $\mathbf{v}_s = K(\mathbf{v}_0 \cos \hat{\alpha} + \mathbf{k} \times \mathbf{v}_0 \sin \hat{\alpha})$.

Subscripts 0 and s denote 1000 mb and surface respectively. $H = H(x, y)$ is the height of the terrain above mean sea level. We have chosen $C_D = 3 \cdot 10^{-3}$, $\rho_s = 1.2923$ kg m^{-3}, $K = 0.7$ and $\hat{\alpha} = \frac{1}{12}\pi$.

Mountains and Ekman friction are thus taken into account.

The lateral conditions are

$$\chi = \omega = \psi_t = 0,$$

$$\frac{\partial \psi}{\partial n} = f^{-1} \frac{\partial \phi}{\partial n} - \oint f^{-1} \frac{\partial \phi}{\partial n} \mathrm{d}n / \oint \mathrm{d}n, \tag{2.8}$$

where n is a coordinate parallel to the lateral boundary. The condition for ψ is adopted from Bolin (1956).

With ϕ given, ψ and χ are easily solved from (2.2), (2.3) and (2.4) with $a = 0$. However, an iteration must be performed between (2.3) and (2.5) due to the Helmholz-term $(f \partial \psi_0 / \partial t)$ in the boundary condition (2.7). FM2 is mathematically very complex and an extensive iteration between (2.2), (2.3), (2.4) and (2.5) is performed with the FM1 fields as initial conditions (Pedersen and Grønskei, 1969). An under-relaxation is applied to secure convergence. The solution of the non-linear balance equation is proved by Iversen and Nordeng (1982) to be straightforward, provided that the geopotential field is adjusted according to the ellipticity condition (Courant and Hilbert, 1962). The maximum adjustments of the height of the 300 mb surface, range between 50 m and 150 m for the different cases. Affected regions are confined to bounded areas with small absolute vorticity, mainly subtropic regions (Paegle and Paegle, 1976).

3. The experiments

To investigate how the different initial fields influence the solution, two primitive equation models are integrated. In model PEM1, the horizontal wind is described by its cartesian components u and v. The equations formulated on a polar stereographic map with map factor m, can be written

$$u_t + m^2 \left[\left(u \frac{u}{m} \right)_x + \left(v \frac{u}{m} \right)_y \right] + (\omega u)_p - (f + \kappa) v + m\phi_x - F_1 = 0, \tag{3.1a}$$

$$v_t + m^2 \left[\left(u \frac{v}{m} \right)_x + \left(v \frac{v}{m} \right)_y \right] + (\omega v)_p + (f + \kappa) u + m\phi_y - F_2 = 0, \tag{3.1b}$$

$$\phi_{pt} + m^2 \left[\left(\phi_p \frac{u}{m} \right)_x + \left(\phi_p \frac{v}{m} \right)_y \right] + \phi_p \omega_p + S\omega = 0, \tag{3.1c}$$

$$\omega_p + m^2 \left[\left(\frac{u}{m} \right)_x + \left(\frac{v}{m} \right)_y \right] = 0, \tag{3.1d}$$

$$(\phi_s)_t + m^2 \left[\left(\phi_s \frac{u_s}{m} \right)_x + \left(\phi_s \frac{v_s}{m} \right)_y \right] + (\omega_s \phi_s)_p = g w_s, \tag{3.1e}$$

with

$$\kappa = m^2 \left[v \left(\frac{1}{m} \right)_x - u \left(\frac{1}{m} \right)_y \right], \quad w_s = v_0 \cdot \nabla H,$$

$$\mathbf{F} = F_1 \mathbf{i} + F_2 \mathbf{j} = -g \partial \boldsymbol{\tau} / \partial p,$$

$$\boldsymbol{\tau} = \begin{cases} \rho_s C_D |\mathbf{v}_s| \mathbf{v}_s \text{ at } p = 1000\,\text{mb} \\ 0 \qquad \text{elsewhere} \end{cases}$$

The finite difference scheme applied to eqs. (3.1) was examined by Grammeltvedt (1969) (scheme F) and he showed that it conserves energy.

The model PEM2 is constructed to obtain a model as consistent with the FMs as possible. Hence, the horizontal equations of motion are the vorticity and the divergence equations with ψ and χ

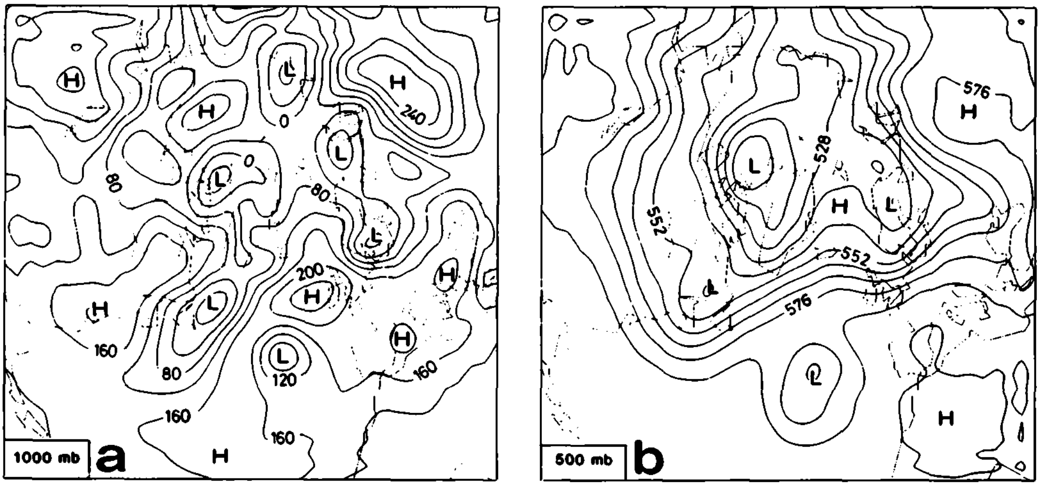

Fig. 1. The geopotential height field obtained after 12 h integration with PEM1 and the Euler backward scheme, i.e. 12 September 1977 00 GMT + 12 h. (a) 1000 mb. (b) 500 mb.

Table 1. *The series of experiments. The initial mass field is a forecast of the geopotential height, 00 GMT 12 September + 12 h, integrated with PEM1 and the Euler backward (EB) scheme. In VIII, the corresponding forecast for the wind is used as initial wind*

Experiment no.	I	II	III	IV	V	VI	VII	VIII
Initial wind	FM1	FM1 no div.	FM2	FM2 no div.	FM1	FM2 no div.	FM2	EB
Model	PEM2	PEM2	PEM2	PEM2	PEM1	PEM1	PEM1	PEM1
No. of timesteps	512	144	512	144	144	144	144	144

as history-carrying variables. The equations are:

$$\nabla^2 \psi_t + (\mathbf{v}_\psi + \mathbf{v}_\chi)\cdot\nabla(\nabla^2\psi + f) + (\nabla^2\psi + f)\,\nabla^2\chi + \omega\nabla^2\psi_p + \mathbf{k}\cdot\nabla\omega \times \frac{\partial \mathbf{v}}{\partial p} - F_\psi = 0, \tag{3.2a}$$

$$\nabla^2\chi_t + \mathbf{v}_\psi\cdot\nabla(\nabla^2\chi) - f\nabla^2\psi + \nabla^2\phi - \nabla f\cdot\nabla\psi + \nabla\cdot(\mathbf{v}_\psi\cdot\nabla\mathbf{v}_\psi) + 2\nabla\cdot(\mathbf{v}_\chi\cdot\nabla\mathbf{v}_\psi) + \nabla\cdot(\omega\mathbf{v}_{\psi_p}) - F_\chi = 0, \tag{3.2b}$$

$$\phi_{pt} + \mathbf{v}\cdot\nabla\phi_p + S\omega = 0, \tag{3.2c}$$

$$\nabla^2\chi + \omega_p = 0, \tag{3.2d}$$

$$\phi_{st} + \mathbf{v}\cdot\nabla\phi_s + \omega_s\,\phi_{sp} = g w_s. \tag{3.2e}$$

In (3.2b), terms containing only χ or ω are omitted as in the balance equation of FM2. Here $F_\psi = -g\partial(\mathbf{k}\cdot\nabla\times\boldsymbol{\tau})/\partial p$ and $F_\chi = -g\partial(\nabla\cdot\boldsymbol{\tau})/\partial p$.

Eqs. (3.2a) and (3.2b) are solved as Poisson equations at each time step. Eqs. (3.1) and (3.2) are solved on a horizontal grid covering a rectangular area on the northern hemisphere of approximately 12,000 km × 11,000 km. The mesh size is $d = 300$ km at 60° N. The filtered models are solved using a non-staggered grid. The same grid is used with the primitive equation models. The vertical area of integration between 200 mb and 1000 mb is resolved in four layers of thickness $\Delta p = 200$ mb with the vertical motion ω computed at the intermediate levels. The boundary conditions are $\omega = 0$ at $p = 200$ mb, and that all time tendencies vanish at the lateral boundaries. To prevent non-linear, numerical instability, a second-order filter (Shapiro, 1970) is applied to the time tendencies at each time step. The time step is $\Delta t = 600$ s.

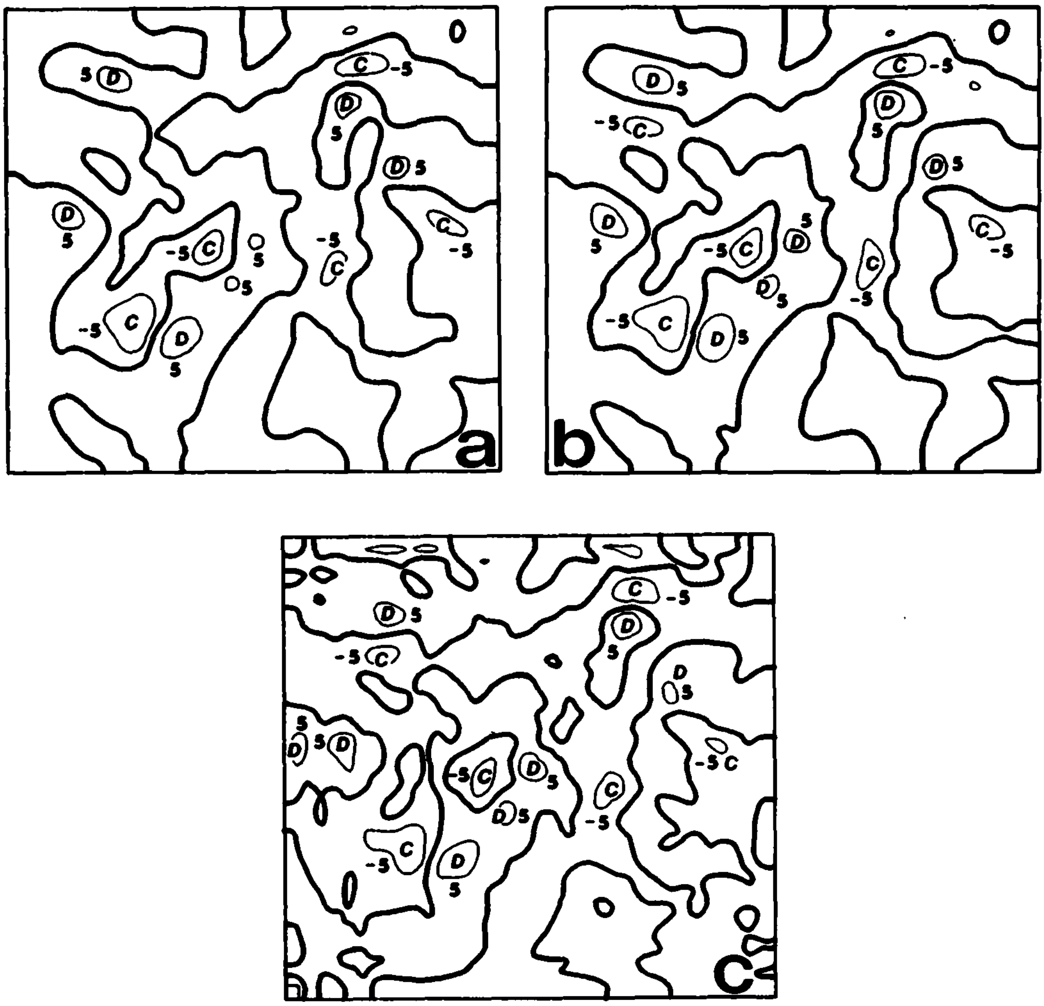

Fig. 2. The horizontal divergence at 12 September 1977 00 GMT + 12 h. Units 10^{-6} s^{-1}. The thick continuous line signifies zero divergence, D indicates divergence and C convergence. (a) FM1, (b) FM2, (c) the field achieved by 12 h integration with PEM1 and the Euler backward scheme.

To get a reference for our results, a 12 h PEM1 forecast was made at 00 GMT 12 September 1977 with FM2 initialization and a Euler backward time scheme. The initial mass field was taken from the routine objective analysis made at the Norwegian Meteorological Institute (Bjørheim, 1979). The resulting forecast for mass field and wind contained very little high-frequency "noise".

The mass field, 12 September 1977, 00 GMT + 12 h displayed in Fig. 1, constitutes the basis for a series of prognostic integrations with the non-damping leap-frog time scheme (see Table 1). The corresponding initial wind is obtained from FM1, FM2 or the Euler backward integration. The differences between FM1 and FM2 are primarily manifested in the horizontal divergence. The divergence of the initial wind fields is shown in Fig. 2. The FM1 and the FM2 divergences are similar, the latter with somewhat larger amplitudes. A closer examination reveals that the divergent part of the FM2 wind is about 10%–25% stronger. The divergence of the wind obtained from the Euler backward integration, resembles that of the filtered models. However, due to the stationarity of waves with wavelength twice the mesh size in a non-staggered grid (Mesinger and Arakawa, 1976), it contains some small-scale energy. In general, stationary waves, for example forced by topography, will not be damped by the Euler backward time scheme.

4. Results

One of the reasons for discussing the schemes presented in this paper is that the horizontal modes are difficult to find. As a consequence, we are not able to decompose a general state of the system into a Rossby mode and a gravity mode. The vertical modes, however, can be found by the method of Økland (1972). The matrix to be diagonalized is in his case symmetric and the eigenvectors are orthogonal. The corresponding eigenvalues are the phase speed of pure gravity waves. They are given in Table 2, while the normalized eigenvectors are displayed in Fig. 3. These eigenvectors do not exactly diagonalize the models PEM1 and PEM2 due to both a horizontally constant static stability and slightly different vertical finite differences. The eigenvectors are found only for the purpose of qualitative discussions. Let $\mathscr{U}$ be the matrix with the eigenvectors as columns. With δ expressing the horizontal wind divergence, the equation of continuity, (3.1d) or (3.2d), can be integrated.

Table 2. *Phase speeds for linear gravity waves in the present four layer model*

Vertical Mode order	Phase speed (m s^{-1})
0	254.9
1	42.6
2	23.5
3	16.2

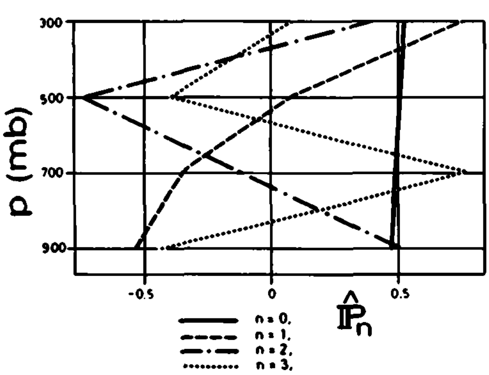

Fig. 3. The normalized vertical eigenvectors $\hat{P}_n$ for linear gravity-inertia waves.

Defining

$$\boldsymbol{\omega} = \begin{pmatrix} \omega_1 \\ \omega_2 \\ \omega_3 \\ \omega_4 \end{pmatrix}, \quad \boldsymbol{\delta} = \begin{pmatrix} \delta_1 \\ \delta_2 \\ \delta_3 \\ \delta_4 \end{pmatrix}, \quad \mathscr{M} = \begin{pmatrix} 1 & 0 & 0 & 0 \\ 1 & 1 & 0 & 0 \\ 1 & 1 & 1 & 0 \\ 1 & 1 & 1 & 1 \end{pmatrix}, \tag{4.1}$$

we have $\boldsymbol{\omega} = -\Delta p \mathscr{M} \boldsymbol{\delta} = -\Delta p \mathscr{M} \mathscr{U} \hat{\boldsymbol{\delta}}$, where

$$\hat{\boldsymbol{\delta}} = \begin{pmatrix} \hat{\delta}_0 \\ \hat{\delta}_1 \\ \hat{\delta}_2 \\ \hat{\delta}_3 \end{pmatrix}$$

is $\boldsymbol{\delta}$ projected into the phase space of the vertical modes and

$$\mathscr{M}\mathscr{U} = \begin{pmatrix} 0.522 & 0.752 & 0.386 & 0.080 \\ 1.030 & 0.841 & -0.358 & -0.327 \\ 1.523 & 0.485 & -0.489 & 0.456 \\ 1.999 & -0.063 & 0.018 & -0.008 \end{pmatrix} \tag{4.2}$$

We now see that ω_4 is clearly dominated by the external mode $\hat{\delta}_0$, while the internal modes are better traced at the upper levels.

In Fig. 4, the absolute values of ω averaged over a central region of the integration area are shown as a function of time for each level. The initial wind is from FM1. For the case of initial divergence included, an almost time-independent development of $\overline{|\omega|}$ is obtained from both PEM1 and PEM2. When initial divergence is omitted, a distinct oscillation about this constant value is excited. This oscillation with a period of about 10 h is hardly traceable at 1000 mb, but is very clear at the upper levels. The oscillation is therefore probably due to an internal gravity-inertia wave, and a look at the time development of ω at a single point indicates the first internal mode. Figures for the case with initial wind from FM2 show very small differences from the curves in Fig. 4. Hence, it is of vital importance that the initial wind contains divergence, and the divergence obtained from FM1 or

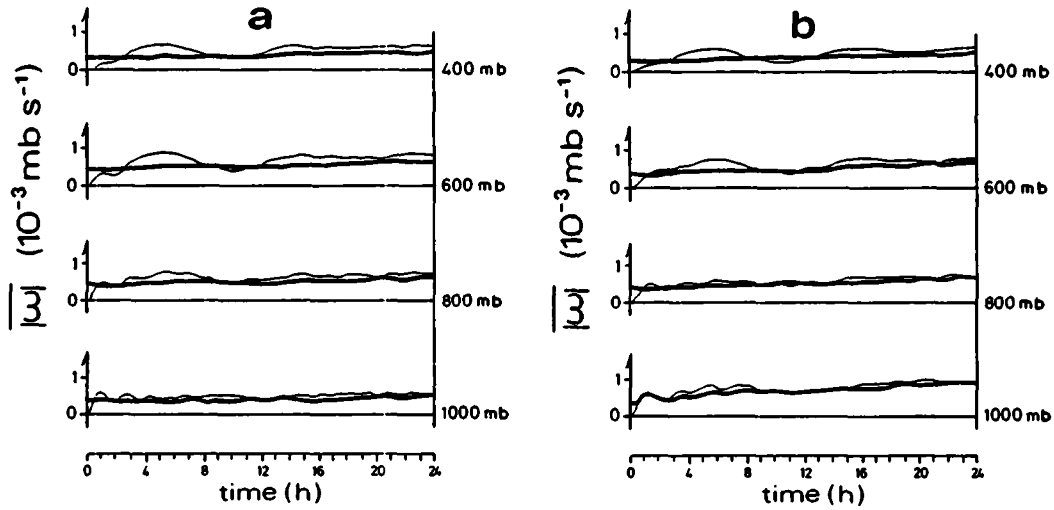

Fig. 4. The area mean of the absolute value of ω versus time. Thick continuous line: with initial divergence; thin continuous line: without initial divergence. (a) Initial wind from FM1 and prognostic model PEM2. (b) Initial wind from FM1 and prognostic model PEM1.

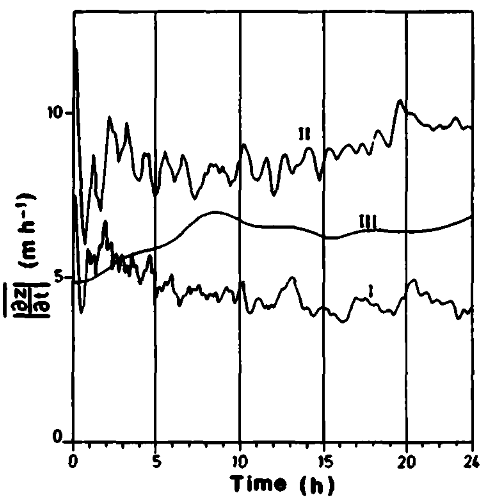

Fig. 5. The area mean of the absolute value of the 1000 mb height tendencies. All tests include initial divergence. Curve I: initial wind from FM2 and prognostic model PEM2. Curve II: initial wind from FM2 and prognostic model PEM1. Curve III: initial wind from the 12 h PEM1 *forecast with Euler backward scheme and* prognostic model PEM1.

FM2 is satisfactory. This contradicts what was found by Lejenäs (1977), but is in accordance with the linear theory of Phillips (1960).

The curves in Fig. 4 also reveal some differences between PEM1 and PEM2 that mainly show up at the 1000 mb level, which indicates the external mode. The PEM1 forecast leads to slowly increasing and distinctly larger values for $\overline{|\omega|}$ at 1000 mb than does the PEM2 forecast. At other levels, differences can hardly be detected. We therefore believe that the inconsistencies in the numerical approximations between the initialization method and the prognostic model give rise chiefly to external gravity-inertia waves. Those waves that are excited due to horizontal finite differences should be of quite short wavelength and hence of high frequency. They are easily eliminated by means of the Euler backward time scheme. In Fig. 5, three curves are displayed showing the area averaged, and absolute geopotential height tendencies at 1000 mb. The curve for PEM1 shows larger values ($\simeq 9$ m h^{-1}) than the PEM2 curves ($\simeq 5$ m h^{-1}), both with initial wind from FM2. The very smooth curve obtained when the Euler backward wind is input for PEM1, is somewhere in between ($\simeq 7$ m h^{-1}), and hence there is some low-frequency energy left in the system. This energy represents either internal modes due to inconsistent vertical differences and interpolations, or an external mode excited by the extrapolation of the wind that has to be made at the lateral boundaries. A test run with an integration area only covering the internal points in the original grid (so that no extrapolation is needed), reveals that the

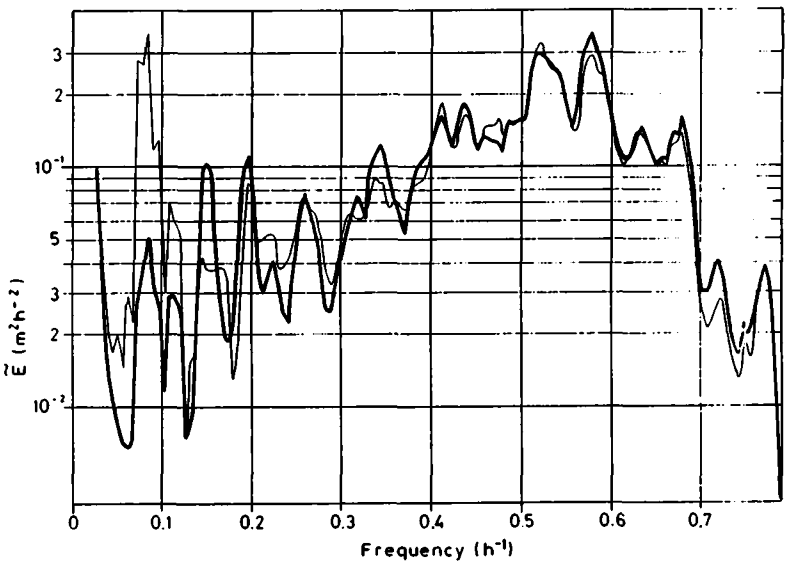

Fig. 6. Averaged energy spectrum of the 1000 mb height tendencies. Prognostic model is PEM2. Thick continuous line: initial wind from FM2. Thin continuous line: initial wind from FM1.

boundary-effects can explain some, but not all, of the energy.

Two of the experiments have been run for a longer time period than the others (512 timesteps). These were forecasts with PEM2, to find differences between the FM1 and FM2 initial fields. We have already mentioned that the development of $\overline{|\omega|}$ for the primitive equation model does not show significant differences. To investigate this further, a Fourier-cosine transformation of the time evolution of the 1000 mb height tendencies was performed. The linear trend of the time series was removed. Subsequent to the application of a frequency smoother, $\tilde{E}_n = (E_{n-1} + E_n + E_{n+1})/3$ ($\nu \cdot \Delta t = n/1024$, ν = frequency, E_n = energy), the energy spectrum was averaged in space. This result is given in Fig. 6. There are very small differences between the two initialization methods, except within the frequency range 0.05 h^{-1}–0.12 h^{-1}, corresponding to a period range 8 h–20 h. Here PEM2 contains considerably more energy when initialized with FM1 than with FM2. Since the main difference between FM1 wind and FM2 wind is their divergence, the low-frequency differences probably trace differences in internal modes.

5. Conclusions

For limited area models on an extratropical region, the non-linear normal mode initialization cannot be applied in a straightforward manner. Other methods are therefore important, In this paper, the classical method of static initialization has been considered, since this method does not require knowledge of the horizontal modes. Two filtered models have been studied; the first, FM1, corresponds to the first iteration in the non-linear, normal mode initialization (Leith, 1980); the second, FM2, assumes the time derivative of the horizontal divergence to vanish. In our case, both FM1 and FM2 produce initial fields that satisfy the demands of non-oscillatory motions, except for some high-frequency energy than can be removed by a time-filtering method. When the prognostic model is not consistent with the filtered, diagnostic model, inconsistencies at the lateral boundaries and in the vertical treatment seem to be the more important. However, the inconsistencies do not lead to fatal developments in our case, but should be paid attention to when using static initialization.

The complete FM2 method give less low-frequency waves. The preference of FM2 will probably be larger for models with more layers or a finer horizontal grid. When solving FM2, an iteration has to be applied. It may be argued that this iteration will not always converge. In some cases the introduction of an under-relaxation coefficient will help, but not always. However, in the non-linear, normal mode initialization there also exist such problems when higher order internal modes are taken into account. These problems are still worse when friction and diabatic affects are included (Temperton and Williamson, 1979). However, a satisfactory balance is achieved by interrupting the iteration after a few scans, even for the divergent cases. In our tests, both topography and Ekman friction are included.

In these tests, mass field constrained initializations are made. If one wishes to include wind observations, a variational technique (Stephens, 1970) or combinations with dynamic initialization methods (e.g. Bratseth, 1982) can be employed.

6. Acknowledgement

This paper was originally a part of the author's joint doctoral thesis at the University of Oslo for which Associate Professor Kaare Pedersen was the scientific adviser. Our appreciation goes to him, and to Mr. Arne Bratseth for valuable discussions. We also want to thank Mr. Anton Eliassen for help in preparing the final version of the paper.

The Norwegian Meteorological Institute partly sponsored the computer time, and the Norwegian Council for Science and the Humanities (NAVF) contributed a fellowship for Trond Iversen (P. No. D. 10-09-018).

REFERENCES

Baer, F. 1977. Adjustment of initial conditions required to suppress gravity oscillations in non-linear flows. *Beitr. Phys. Atmos. 50*, 350–366.

Baer, F. and Tribbia, J. J. 1977. On complete filtering of gravity modes through non-linear initialization. *Mon. Wea. Rev. 105*, 1536–1539.

Bjørheim, K. 1979. The objective analysis scheme for operational use at the Norwegian Meteorological Institute. Technical report no. 40. The Norwegian Meteorological Institute, Oslo, Norway.

Bolin, B. 1956. An improved barotropic model and some aspects of using the balance equation for three-dimensional flow. *Tellus 8*, 61–75.

Bratseth, A. M. 1982. A simple and efficient approach to the initialization of weather prediction models. *Tellus 34*, 352–357.

Charney, J. G. 1955. The use of primitive equations of motion in numerical prediction. *Tellus 7*, 22–26.

Courant, R. and Hilbert, D. 1962. *Methods of mathematical physics*. Vol. 2. Interscience Publishers, New York, 324–326.

Daley, R. 1978. Variational non-linear normal mode initialization. *Tellus 30*, 201–218.

Grammeltvedt, A. 1969. A survey of finite-difference schemes for the primitive equations for a barotropic fluid. *Mon. Wea. Rev. 97*, 384–404.

Hinkelmann, K. 1951. Der Mechanismus des meteorologischen Lärmes. *Tellus 3*, 285–296.

Houghton, D. D. and Washington, W. 1969. On global initialization of the primitive equations. *J. Appl. Meteorol. 8*, 726–737.

Iversen, T. and Nordeng, T. E. 1982. A convergent method for solving the balance equation. *Mon. Wea. Rev. 110*, 1347–1353.

Leith, C. E. 1980. Non-linear normal mode initialization and quasi-geostrophic theory. *J. Atmos. Sci. 37*, 958–968.

Lejenäs, H. 1977. Initialization of primitive equation models—Some aspects of including a divergent wind component into the initial state. *Beitr. Phys. Atmos. 50*, 154–168.

Lorenz, E. N. 1960. Energy and numerical weather prediction. *Tellus 12*, 364–373.

Machenhauer, B. 1977. On the dynamics of gravity oscillations in a shallow water model with application to normal mode initialization. *Beitr. Phys. Atmos. 50*, 253–271.

Mesinger, F. and Arakawa, A. 1976. Numerical methods used in atmospheric models. Vol. 1. *GARP Publication Series, 17*, WMO, Geneva.

Miyakoda, K. and Moyer, R. W. 1968. A method of initialization for dynamical weather forecasting. *Tellus 20*, 115–128.

Nitta, T. and Hovermale, J. B. 1969. A technique of objective analysis and initialization for the primitive forecast equations. *Mon. Wea. Rev. 97*, 652–658.

Økland, H. 1972. On the balance, initialization and data assimilation in primitive equation prediction models. *J. Atmos. Sci. 29*, 641–648.

Paegle, J. and Paegle, J. N. 1976. On geopotential data and ellipticity of the balance equation: a data study. *Mon. Wea. Rev. 104*, 1279–1288.

Pedersen, K. and Grønskei, K. E. 1969. A method of initialization for dynamical weather forecasting and a balanced model. *Geophys. Norv.* No. 7.

Phillips. N. A. 1960. On the problem of initial data for the primitive equations. *Tellus 12*, 121–126.

Shapiro, R. 1970. Smoothing, filtering and boundary effects. *Rev. Geophys. Space Phys. 8*, 359–387.

Stephens, J. J. 1970. Variational initialization with the balance equation. *J. Appl. Meteorol. 9*, 732–739.

Temperton, C. and Williamson, D. L. 1979. Normal mode initialization for a multi-level gridpoint model. ECMWF Technical Report No. 11.

Tribbia, J. J. 1979. Non-linear initialization on an equatorial β-plane. *Mon. Wea. Rev. 107*, 704–713.

Tribbia, J. J. 1981. Non-linear normal mode balancing and the ellipticity condition. *Mon. Wea. Rev. 109*, 1751–1761.